ASME Journal of Turbomachinery
Online journal at:
https://asmedigitalcollection.asme.org/turbomachinery

Samuel Altland
Department of Mechanical Engineering,
The Pennsylvania State University,
University Park, PA 16802
e-mail: sja198@psu.edu

Xiang I. A. Yang
Department of Mechanical Engineering,
The Pennsylvania State University,
University Park, PA 16802
e-mail: xzy48@psu.edu

Karen A. Thole
Department of Mechanical Engineering,
The Pennsylvania State University,
University Park, PA 16802
e-mail: kat18@psu.edu

Robert Kunz[1]
Department of Mechanical Engineering,
The Pennsylvania State University,
University Park, PA 16802
e-mail: rfk102@psu.edu

Stephen McClain
Department of Mechanical Engineering,
Baylor University,
Waco, TX 76706
e-mail: Stephen_McClain@baylor.edu

Application of a Distributed Element Roughness Model to Additively Manufactured Internal Cooling Channels

Design for cooling effectiveness in turbine blades relies on accurate models for dynamic losses and heat transfer of internal cooling passages. Metal additive manufacturing (AM) has expanded the design space for these configurations, but can give rise to large-scale roughness features. The range of roughness length scales in these systems makes morphology resolved computational fluid dynamics (CFD) impractical. However, volumetric roughness models can be leveraged, as they have computational costs orders of magnitude lower. In this work, a discrete element roughness model (DERM), based on the double-averaged Navier–Stokes equations, is presented and applied to additively manufactured rough channels, representative of gas turbine blade cooling passages. Unique to this formulation of DERM is a generalized sheltering-based treatment of drag, a two-layer model for spatially averaged Reynolds stresses, and explicit treatment of dispersion. Six different AM rough surface channel configurations are studied, with roughness trough to peak sizes ranging from 15% to 60% nominal channel passage half-width, and the roughness Reynolds number ranges from $Re_k = 60$ to 300. DERM predictions for spatially and temporally averaged mean flow quantities are compared to previously reported direct numerical simulation results. Good agreement in the mean velocity profiles, stress balances, and drag partitions are observed. While DERM models are typically calibrated to specific deterministic roughness morphologies at comparatively small roughness Reynolds numbers, the present more generalized DERM formulation has wider applicability. Here, it is demonstrated that the model can accommodate random roughness of large scale, typical of AM.
[DOI: 10.1115/1.4062838]

Keywords: computational fluid dynamics (CFD), heat transfer, film cooling

1 Introduction

The growth of additive manufacturing (AM) has significantly expanded the design space for gas turbine blade cooling geometries. As this technology has matured, an entirely new class of complex cooling passages are now possible, which could allow for higher operating temperatures and thereby improved engine efficiency.

However, AM gives rise to an entirely new class of large-scale surface roughness, that by the nature of the manufacturing process, cannot be removed with postprocessing. Characterization and measurements of the drag and heat transfer augmentation induced by this class of AM surfaces is an active area of research. Snyder et al. [1,2], Stimpson et al. [3,4], and Kirch and Thole [5] have investigated various aspects of engine-scale AM internal cooling channels, including the influence of build direction, geometric tolerances, and surface roughness correlations.

In order to successfully leverage the opportunities of AM, designers require analysis tools that allow for the efficient, yet accurate prediction of the aero-thermal properties of these surfaces. Due to the high overhead costs and limited bandwidth of experimental investigation, computational fluid dynamics (CFD) remains the primary predictive method for rough wall turbulent boundary layers. Directly resolving a rough surface using body fitted grids presents its own set of challenges due to the disparate length scales present. Capturing both the near-wall viscous region and resolving the roughness elements themselves in both the streamwise and transverse directions drive up cell count dramatically compared to a smooth-wall case. For an AM channel, the required cell count can rise into the tens of millions [6], which is impractical from a design perspective.

Surface parameterizations of roughness such as k^+-based sand grain roughness (SGR) models are considerably cheaper to implement due to the use of smooth-wall grids. However, their simplicity makes them a far less-flexible tool to accommodate the wide range of possible surface roughness fields. First, a surface's k_s value must be obtained from either experimental investigation or direct numerical simulation (DNS) and is not known a priori. Additionally, while many efforts have been made over the years to create robust

[1]Corresponding author.

Contributed by the International Gas Turbine Institute (IGTI) of ASME for publication in the Journal of Turbomachinery. Manuscript received December 30, 2022; final manuscript received June 20, 2023; published online July 28, 2023. Tech. Editor: David G. Bogard.

correlations between actual surface statistics and k_s, these are far from universal [7,8]. Investigations have shown that roughness RMS height, element skewness, kurtosis, and sheltering all interact in a complex way to determine drag, and that modification of the turbulent boundary layer cannot be condensed to a single-length scale [9,10].

An alternative to surface parameterization of the roughness field is volumetric parameterization, a concept that dates back to Schlicting [11]. A subset of these approaches is discrete element roughness model (DERM). In the DERM approach, the governing equations are spanwise spatially averaged (i.e., tangent to the wall), so the explicit geometry of the roughness is averaged away. The influence of surface roughness on the flow is represented in closure terms that appear in the averaged equations, which represent interfacial forces, dispersion, and Reynolds stresses due to space and time averaging. The roughness field itself is represented by wall-normal volume fraction and volume fraction gradient distributions. DERM has the advantage of the low computational cost associated with smooth-wall grids (like SGR models), while accommodating the geometric richness of complex roughness morphologies. This comes at the cost of requiring a suitable representation of the roughness element volume fraction field and robust closures for the averaged Navier–Stokes equations.

Taylor et al. [12–14] were the first to rigorously derive a DERM model using control volume analysis, and the resulting two-dimensional time-averaged boundary layer equations served as the starting point for future efforts. Significant improvements were made to Taylor's model by McClain et al., who extended Taylor's model to random roughness, modified the existing drag term, and identified useful parameterization methods for rough surfaces [15–17]. Aupoix [18] endeavored to construct a more general model for DERM through a double averaging (both time and space) of the Navier–Stokes equations. This spatial averaging technique is widely used in the porous media field [19–21]. After revisiting his model, Aupoix [22] identified that in addition to the traditional Reynolds stress term and drag effort term, the spatial averaging gives rise to a term that contains the product of spatially fluctuating velocity components, otherwise known as the dispersive stress. While Aupoix did not attempt to provide closure for all terms that appear in the exact averaged equations, his review provided insight into many of the challenges involved in fully implementing this generalized DERM and also serves as a comprehensive literature survey of the field.

Hanson et al. derived double-averaged equations for the compressible flow, with a specific focus on the heat transfer on ice-roughened airfoils [23–25]. Hanson's work was one of the first to attack the double-averaged energy equation and the attendant closure terms, and implement the DERM equations in the context of a general finite volume CFD solver. Chedevergne and Forooghi [26] published the ONERA formulation of DERM, which combines Aupoix double averaged incompressible equations, a mixing length turbulence model, a modified varying sectional drag coefficient, and McClain's meltdown height approach, which was validated against DNS of cone-like surrogate roughness.

The goal of this article is to demonstrate the applicability of a new DERM formulation to an important class of surface roughness. In particular, we apply this DERM to channels with random roughness comparable to the channel height, as arises in AM turbine blade cooling passages. These channels have recently been explored both experimentally and computationally by Snyder et al. [1], Stimpson et al. [4], Hanson et al. [6], McClain et al. [27], Stafford et al. [28], and Altland et al. [29]. Unique to this formulation of DERM is a generalized treatment of the DERM drag force and the spatially averaged Reynolds stresses. This work proposes a spatially varying sectional drag coefficient, which is determined by invoking so-called sheltering theory. This generalized formulation of the drag coefficient allows for improved model accuracy across a wider array of potential roughness fields, without having to rely on calibration for each morphology. A novel two-layer approach to modeling the spatially averaged Reynolds stress is also proposed.

The remainder of the article is organized as follows. First, the different geometric configurations investigated are described, and the details of the proposed DERM model are discussed. Then, results from a series of numerical studies on AM rough channels are compared to our groups previously reported DNS. Finally, an assessment of the predictive capabilities of the DERM model are given, and recommendations for model improvement are made.

2 Technical Approach

2.1 Roughness Configurations and Characterization. This study considers three different rough surface topologies, which are all computed tomography (CT) scans of additively manufactured surfaces. These surfaces are referred to as *upskin*, *downskin*, and *real*. Further details of the three rough surfaces can be found in the study by Stafford et al. [28] and McClain et al. [27], where they are referred to by the same names. The *upskin* and *downskin* surfaces were manufactured with Inconel 718 and the *real* surface with Hastelloy. We place each rough surface opposite a smooth surface and the other two rough surfaces. This leads to six-channel configurations. Table 1 lists details of these rough wall channels. The case ID nomenclature is bottom-surface/top-surface, with designations *upskin* (u), *downskin* (d), *real* (r), and smooth (s).

Figure 1 is a sketch of a rough wall channel configuration at a given spanwise location. Here, x is the streamwise direction, z is the wall-normal direction, δ is the half-channel height, and L_z is the channel height. In all six cases, $L_z = 2\delta$, which is measured from the underlying substrate of the bottom wall, to the substrate of the top wall. The bottom wall roughness extends from 0 to a peak height $k_{b,\max}$, and the top wall roughness extends from L_z down to a peak height of $k_{t,\max}$. The average heights of the bottom and top walls are $k_{b,m}$ and $k_{t,m}$ respectively. From Table 1, it should be clear that these rough surfaces obstruct a significant part of the channel, and the maximum extent of the roughness is comparable to the half-channel height in all cases; indeed, $k_{\max}/\delta \approx \frac{2}{3}$ for the *real* surface.

We can define a wall normal distribution of volume fraction β, such that $\beta = \forall_f/\forall$, the ratio of fluid-to-total planar area at a given elevation. Above the maximum extent of the roughness, $\beta = 1$, as there is no obstruction of the fluid, and $\beta < 1$ below $k_{\max}$. The roughness height distribution is close to Gaussian for all three AM surfaces [29]. Accordingly, the wall normal

Table 1 Roughness configurations

Case ID	$k_{b,\max}/\delta$	$k_{t,\max}/\delta$	$\mathrm{Re}_{\tau,N}$
u/s	0.155	0	410
d/s	0.404	0	431
r/s	0.667	0	474
u/d	0.142	0.390	446
u/r	0.130	0.646	495
d/r	0.341	0.620	510

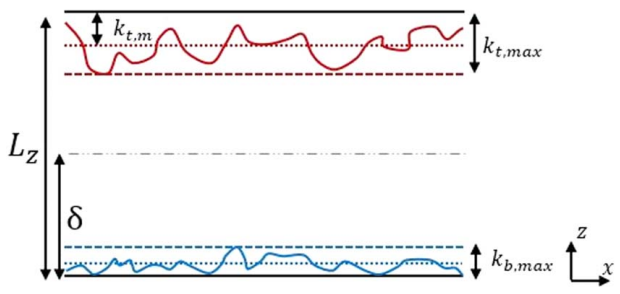

Fig. 1 Rough wall channel sketch with nomenclature

distribution of volume fraction can be written analytically as the cumulative density function of the roughness height and is given by Eq. (1) and plotted in Fig. 2.

$$\beta(z) = \frac{1}{2}\left[1 + erf\left(\frac{z - k_m}{\sigma_k\sqrt{2}}\right)\right] \tag{1}$$

2.2 DERM Equations and Model Closures. The governing equations for DERM are derived by spatially and temporally averaging the Navier–Stokes equations. This double-averaging procedure is reviewed in the study by Aupoix [22]. Just as in Reynolds averaging, where flow variables are decomposed into temporally averaged and temporally fluctuating components using $\phi = \overline{\phi} + \phi'$, spatial averaging requires decomposition into spatially averaged and spatially fluctuating terms, where $\phi = \langle\phi\rangle^f + \phi''$. In this notation, $\bar{\cdot}$ denotes time averaged, $\cdot'$ denotes temporal fluctuations, and $\cdot''$ denotes spatial fluctuations. $\langle\cdot\rangle^f$ denotes an intrinsic spatial average, and $\langle\cdot\rangle$ denotes comprehensive spatial averaging. These two volume averages are related through $\langle\phi\rangle = \beta\langle\phi\rangle^f$.

For conciseness, we present the model here for fully developed periodic channel flow. In practice, the model is applied within conventional 3D sublayer-resolved Reynolds-averaged Navier–Stokes (RANS). Accordingly, the fully developed incompressible DERM x-momentum equation is given by

$$\frac{\partial}{\partial z}\left(\nu\frac{\partial\beta\langle\overline{U}\rangle^f}{\partial z} - \langle\overline{u'w'}\rangle - \langle u''w''\rangle\right) - \frac{1}{\rho}\frac{\partial\langle\overline{p}\rangle}{\partial x} + f_D = 0 \tag{2}$$

where ν is the kinematic viscosity, p is the pressure, and U is the streamwise velocity. The terms from left to right are viscous diffusion, turbulent transport, dispersive stress, pressure gradient, and f_D is the drag effort term.

In this formulation of DERM, the primary variable of interest is the double-averaged streamwise velocity $\langle\overline{U}\rangle$. DERM does not provide details of the spatially resolved velocity field, but the local contributions to the momentum balance are embodied in the modeled stress terms. Prediction of the double-averaged velocity, and thereby skin friction, is generally sufficient for flow characterization, making DERM useful as a design level tool.

Equation (2) is a fairly universal starting point for DERM. In order to close the DERM momentum equation, the drag effort term, the spatially averaged Reynolds stress, and the dispersive stress all require modeling. Our treatment of each of the these terms is detailed in the following sections.

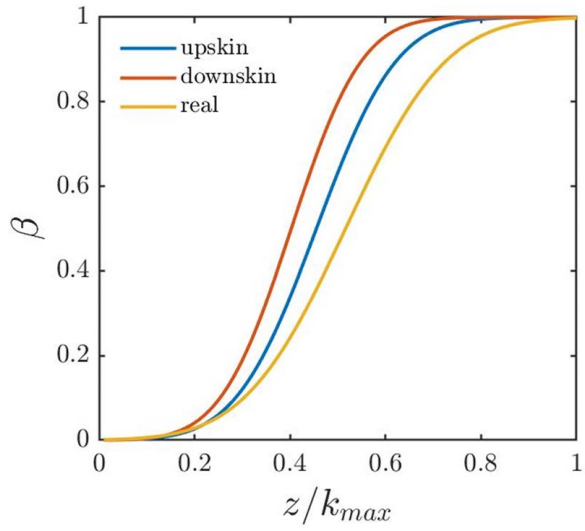

Fig. 2 Wall normal volume fraction distribution

2.2.1 Drag Closure. Closure of the drag term has historically been the most active area of DERM research. The majority of DERM models use a general convective drag law, given by Eq. (3) to model the momentum sink imposed by the surface roughness on the fluid.

$$f_D = -\frac{\frac{1}{2}C_D A_f(\langle\overline{U}\rangle^f)^2}{\forall} \tag{3}$$

Here, A_f is the projected frontal area of the roughness. For the deterministic roughness fields that have historically been the target of DERM modeling, such as hemispheres or cones, the frontal area projection can be written in terms of the characteristic diameter of the roughness element and an element spacing parameter. For the roughness in this study, the average frontal area per unit planar area as a function of z can be determined by directly interrogating the CT scans.

The sectional drag coefficient is the challenging feature, and a considerable amount of variation is seen in the form of C_D among authors. Historically, the drag coefficient was curve fit from a suite of experimental data (see Taylor et al. [14] and Chedevergne and Forooghi [26]). However, this limited the applicability of the model to roughness fields that were similar in morphology to the calibration case. As an alternative, we have turned to sheltering theory to develop a more generalized drag coefficient.

Flow sheltering is a concept that was introduced into the roughness literature by Raupach [30]. Its main perspective is that a roughness element in the wake of another roughness element exerts less drag force on the flow than if it were fully exposed to the incoming fluid. Yang et al. [31] developed a fully analytical sheltering model for the effective drag exerted on an arbitrary rough surface. There, the average velocity in a rough wall turbulent boundary layer is written as the sum of two shape functions, an exponential profile in the roughness occupied region, and a logarithmic profile above the roughness height. Equation (4) gives the form of these shape functions.

$$U(z) = \begin{cases} U_k \exp^{\frac{a(z-k_{\max})}{k_{\max}}} & \text{if } 0 < z < k_{\max} \\ \frac{u_\tau}{\kappa}\log\frac{z-d}{z_o} & \text{if } k_{\max} < z < H \end{cases} \tag{4}$$

To completely describe the average velocity field $U(z)$, five unknown constants must be solved for: the velocity attenuation parameter a, the displacement height d, the roughness length scale z_o, the friction velocity u_τ, and U_k, the velocity at $k_{\max}$. Five constraints are therefore required. Four of these are force balance (integrated skin friction equal to integrated form drag), velocity continuity at $z = k_{\max}$ and $z = H$, and the formal definition of d (centroid height of the distributed drag force). Here, H is the boundary layer height.

The fifth constraint and a novel contribution from Yang et al. is a method for determining a, which is a measure of flow sheltering. It is an intuitive that the attenuation parameter should be dependent on the geometric configuration, and that it should increase the more densely packed the roughness elements are. The sheltering model in Ref. [31] characterizes the wake interactions of an arbitrary roughness geometry by returning the attenuation parameter a. With this final constraint, all five constants in Eq. (4) can be evaluated and a full prediction of $U(z)$ is obtained. Further details of the sheltering approach can be found in Ref. [31] and are not presented here for brevity.

In the context of DERM, the exponential shape function for the average velocity in the roughness occupied region is used to define a sectional drag coefficient as a function of wall normal coordinate.

$$C_D(z) = C_o e^{-\frac{(a-a_o)(z-k_{\max})}{k_{\max}}} \tag{5}$$

Here, C_o is the drag coefficient of an isolated roughness element and a_o is the minimum attenuation coefficient. The minimum attenuation coefficient estimates the attenuation in the sparse roughness limit, and a value of $a_o = .4$ is used. $C_o \approx \mathcal{O}(1)$ can be obtained

from the literature for many deterministic roughness shapes. We take $C_o = 1$ here, as justified by the force balance predictions shown in Sec. 3. In the limit of very sparsely packed roughness, $a \to a_o$ and this model returns the isolated drag coefficient. The benefit of this sheltering approach is that it can accommodate a wide variety of topologies and is independent the calibration that classic DERM drag coefficients rely upon.

2.2.2 Spatially Averaged Reynolds Stress. In addition to the drag term, special treatment of the spatially averaged Reynolds stress term in Eq. (2) is required for DERM closure. Unfortunately, using spatially averaged versions of the RANS turbulence model equations to calculate an average eddy viscosity ν_τ presents several challenges. These include a large number of unclosed co-variances and ambiguity related to the boundary conditions for these equations. As a consequence, mixing length turbulence models have been the primary method of closing the averaged Reynolds stress in DERM [26,32], i.e.,

$$\langle \overline{u'w'} \rangle = \nu_\tau \frac{\partial \beta \langle \overline{U} \rangle^f}{\partial z}$$
$$\nu_\tau = l_m^2 \frac{\partial \beta \langle \overline{U} \rangle^f}{\partial z} \tag{6}$$

The exact form of the mixing length both above and below the roughness height is another area where divergent approaches have been used in the DERM community. In this work, we adopt a hybrid eddy viscosity approach, with a conventional DERM mixing length formulation blended with an outer region two equation RANS turbulence model.

The mixing length expression employed in this work has two layers. $l_{m,o}$ is the form of the mixing length above the extent of the roughness $k_{\max}$, and $l_{m,i}$ is used in the roughness occupied region.

$$l_{m,o} = \left[(\delta - d)\left(0.14 - 0.08\hat{z}^2 - 0.06\hat{z}^4\right) \right] f_{\text{VanD}}$$
$$f_{\text{VanD}} = 1 - e^{\frac{-u_{\tau,T}(z-d)}{26\nu}}$$
$$l_{m,i} = l_{m,o}|_{k_{\max}} \left[1 - \tanh\left(\frac{k_{\max} - z}{k_{\max}} \right) \right] \frac{z}{k_{\max}} \tag{7}$$

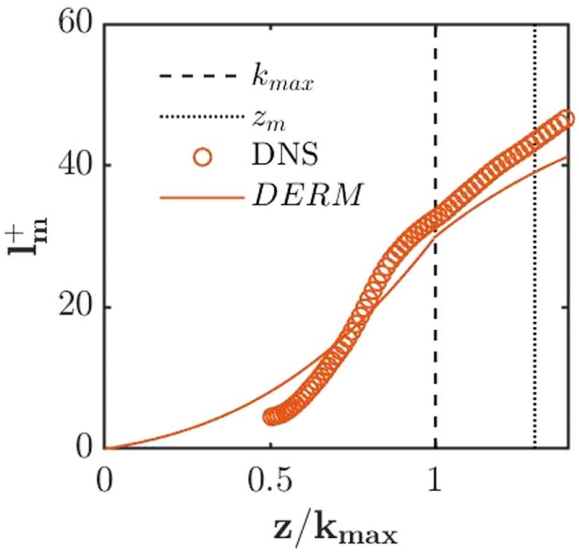

Fig. 3 Mixing length $l_m(z)$ for d/s. The colored solid line is the proposed closure expression for DERM. Symbols are calculated from DNS. The location of the maximum roughness height $k_{\max}$ and blending height z_m are also included.

The variable $\hat{z} = \left(1 - \frac{z-d}{\delta - d}\right)$ is a corrected wall distance. Here, d is the displacement and $u_{\tau,T}$ is the total friction velocity (see Sec. 2.3). The mixing length above the roughness $l_{m,o}$ is a modified version of the smooth-wall turbulent internal flow expression derived by Nikuradse [33] and validated by Antonialli and and Silveira-Neto [34]. Here, the expression has been corrected by the displacement height d, to account for the fact that the roughness takes up a non-negligible portion of the channel. The value of d used in the mixing length model is obtained from the sheltering model as discussed in Sec. 2.2.1. For the present set of additive surfaces, the displacement height is approximately equal to k_m. This outer layer form has been used previously in the context of DERM [26]. The inclusion of the Van Driest damping expression f_{VanD} is to accommodate the smooth-wall limit where both $k_{\max}$ and d are zero, i.e., to recover the traditional mixing length expression.

The mixing length below the height of the roughness ($l_{m,i}$) blends the outer mixing length down to 0 at the underlying substrate. Here, a hyperbolic tangent is used to damp the mixing length, and this expression was informed by interrogation of our DNS data [29]. In particular, this function was chosen in an attempt to match the DNS mixing length in the upper half of the roughness occupied region, since the assumptions of mixing length models break down deep within the roughness occupied layer. This model returns Reynolds stresses with reasonable accuracy all the way down to the substrate, as shown in Sec. 3. Figure 3 shows the mixing length expression given by Eq. (7) compared to the DNS data for the *d/s* case. Good agreement is observed for the upper part of the roughness occupied region and above the roughness.

A pure mixing length approach like those taken in other DERM models would require additional smoothing or blending to accommodate nonsymmetrically rough channels, as arise in this study and AM cooling channels in general. In order to avoid discontinuities in the mixing lengths from both the top and bottom walls, we propose a two-layer formulation for the eddy viscosity in the channel. Below a blending height z_m, which we set as $1.3k_{\max}$ (or 0.25δ for smooth walls), the eddy viscosity for Eq. (6) is calculated using the previously described mixing length model. Above z_m, ν_τ is calculated using the $k - \varepsilon$ turbulence model [35]. In order to ensure continuity across the match location, the k transport equation is also solved in the mixing length region, and ε is directly computed from the values of k and ν_τ: $\varepsilon = C_\mu k^2/\nu_\tau$. These values of k and ε then act as boundary conditions on the outer region, ensuring continuity of eddy viscosity. Validation of this proposed approach is shown in Sec. 3. Additionally, this two-layer approach retains the generality of freestream turbulence condition transport.

2.2.3 Dispersive Stress. The final term in Eq. (2) that requires discussion is the dispersive stress. Just as Reynolds stress arises from the temporal averaging of the convection term in the momentum equation, dispersive stress arises from the spatial average and analogously represents the product of unresolved spatial fluctuations in velocity. While this term has long been identified both within and outside of the DERM community, little effort has been undertaken to explicitly model it. For many roughness morphologies, the magnitude of dispersive stress is small compared to the Reynolds stress [36–38]. However, for the AM surfaces considered in this study, dispersion can represent a significant fraction of the total stress budget and therefore should be accounted for.

Machine learning has been explored by numerous researchers within the context of CFD and has been employed in instances where lack of knowledge about the underlying physics complicates the development of closure models [39]. Here, we use a data-based approach, namely, a feedforwrad neural network, to model the dispersive stress. The neural network inputs I and output O are given in Eq. (8).

$$I = \left[\frac{z}{k_{\max}}, \frac{k_m}{k_{\max}}, \frac{k_{\text{rms}}}{k_{\max}}, k_{\text{krt}}, \frac{-\nu \frac{\partial \langle U \rangle}{\partial z}}{u_{\tau,T}^2}, \text{ES} \right], \quad O = \frac{<u''w''>}{u_{\tau,T}^2} \tag{8}$$

Here, the six inputs to the network are the wall normal coordinate z, the mean roughness elevation k_m, the root-mean-squared roughness height k_{rms}, the kurtosis of the roughness distribution k_{rms}, the local velocity gradient, and the roughness element slope ES. The output is one value, the local dispersion. These input quantities were chosen for several reasons. First, the roughness statistics used here are among the most commonly reported in surface characterization for both random and deterministic surfaces [40]. Second, the velocity gradient is included as an input to allow dynamic feedback in the system.

The neural network employs 1 hidden layer with 40 nodes. The network was trained using a combination of the DNS in Ref. [29] and DNS of cube array roughness [41]. The Levenberg–Marquardt [42] algorithm was used for network optimization. The weights and biases of the trained network are encoded into the CFD solver, such that in every computational cell, the network inputs are supplied, and a local value of dispersion is obtained (see Ref. [43] for further details on dispersive stress modeling).

2.3 Computational Details. This DERM model has been implemented using NPHASE-PSU [44], an in-house finite volume multiphase code. The domain is discritized using a sublayer-resolved mesh, with comparable wall-normal resolution to DNS. Unlike other DERM models, this formulation does not use the melt down height as the reference datum and instead uses the underlying substrate of the bottom wall roughness. As is often done in DNS, we can eliminate the pressure gradient term in Eq. (2) in deference to a volumetric body force f_b, such that $\frac{\partial \langle \overline{p} \rangle}{\partial x} = \beta f_b$. The flow is driven by a constant volumetric body force f_b, which has units of N/m^3, for all six cases.

In order to consistently compare our DERM results to DNS, while also presenting self-consistent law-of-the-wall-comparisons, we require two definitions of the friction velocity. The *nominal* friction velocity $u_{\tau,N}$ and total friction velocity $u_{\tau,T}$ are given by Eq. (9).

$$u_{\tau,N} = \sqrt{\frac{f_b \delta}{\rho}}, \quad u_{\tau,T} = \sqrt{\nu \frac{\partial \langle U \rangle}{\partial z}|_{z=k_{\min}} + \int_{k_{\min}}^{k_{\max}} f_D \, dz} \tag{9}$$

We scale the problem such that $u_{\tau,N}$ is constant for all six cases and vary the kinematic viscosity to achieve the desired nominal Reynolds number, $\text{Re}_{\tau,N} = u_{\tau,N}\ \delta/\nu$, and roughness Reynolds number, $\text{Re}_k = u_{\tau,N}\ k_{\max}/\nu$. This approach is identical to the one taken in the DNS study [29]. Values of $\text{Re}_{\tau,N}$ are listed in Table 1. For the surfaces considered in this study, the roughness Reynolds numbers range from $\text{Re}_k \approx 60$ to 300.

The total friction velocity $u_{\tau,T}$ is a unique quantity for each rough wall. For the DERM simulations, $u_{\tau,T}$ is calculated based upon each rough wall's contribution to the total drag force. This drag force is the sum of both the drag on the roughness elements embodied by the effort term f_D, and the viscous drag on the underlying substrate. The limit k_{min} is the coordinate of the underlying substrate, which is $z = 0$ for the bottom wall and $z = L_z = 2\delta$ for the top wall.

3 Results

In this section, we present the results of the proposed DERM model when applied to the six rough surface configurations. The DNS results used for comparison are of identical channel geometries. The DNS were conducted using the in-house code LESGO to solve the incompressible Navier–Stokes equations. The code uses a spectral method for spatial discretization in the streamwise and spanwise directions, and a second-order finite difference method in the wall normal direction. A second-order Adam–Bashforth method was used for time advancement, and statistically converged results were temporally and spatially averaged to allow for direct comparison with the DERM predictions. Full details of the DNS can be found in the study by Altland et al. [29].

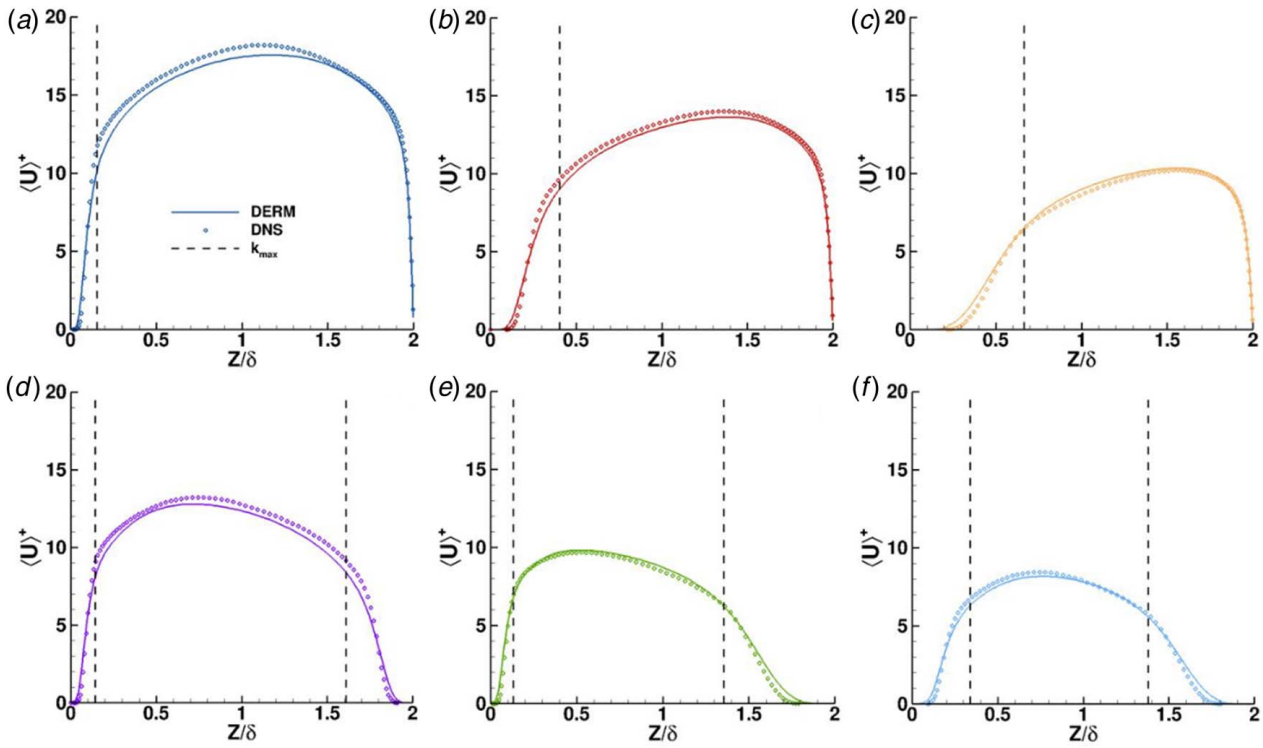

Fig. 4 Double-averaged velocity profiles for the six roughness configurations: (*a*) u/s, (*b*) d/s, (*c*) r/s, (*d*) u/d, (e) u/r, and (*f*) d/r. Solid lines are DERM profiles. Symbols are DNS. Black dashed lines indicate the maximum height of the roughness. Normalization by $u_{\tau,N}$.

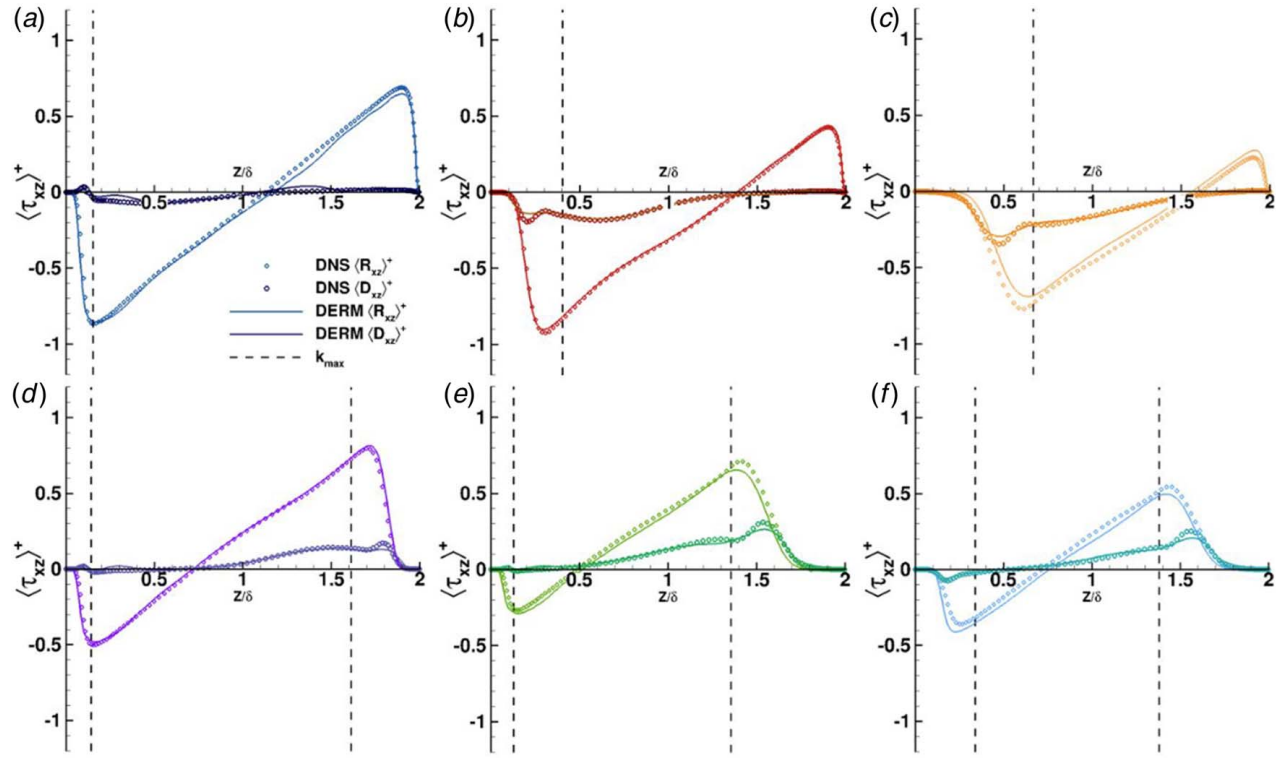

Fig. 5 Double-averaged stress profiles for the six roughness configurations. (*a*) u/s, (*b*) d/s, (*c*) r/s, (*d*) u/d, (*e*) u/r, and (*f*) d/r. Light solid lines are DERM profiles of R_{xz}^+ [$\langle \overline{u'w'} \rangle^+$]. Dark solid lines are DERM profiles of D_{xz}^+ [$\langle u''w'' \rangle^+$]. Diamond symbols are DNS profiles of R_{xz}^+. Circle symbols are DNS profiles of D_{xz}^+. Black dashed lines indicate the maximum height of the roughness. Normalization by $u_{\tau,N}^2$.

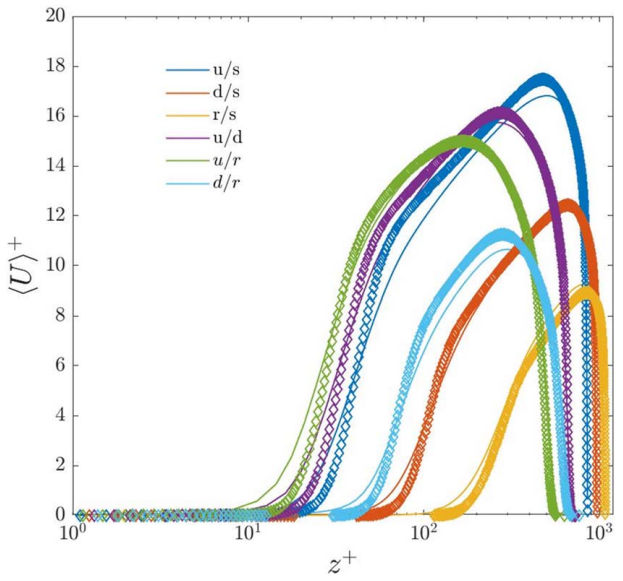

Fig. 6 Double-averaged DERM velocity profiles for the bottom walls for all six cases. Normalization by $u_{\tau,T}$. Solid lines are DERM, and symbols are DNS.

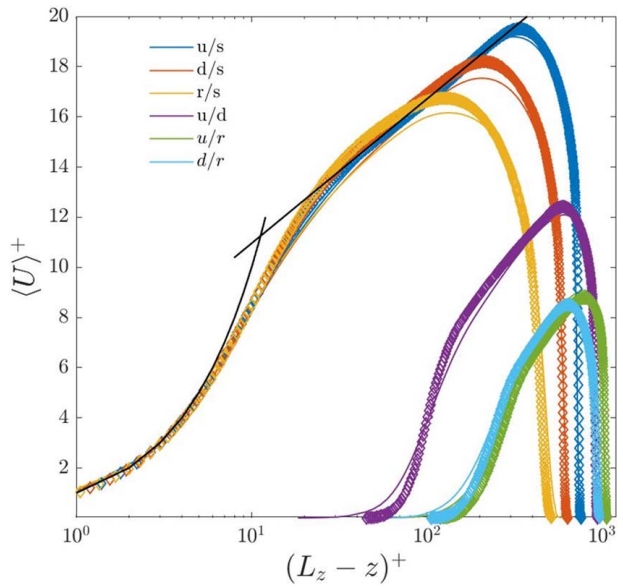

Fig. 7 Double-averaged DERM velocity profiles for the top walls for all six cases. Black solid lines are the law-of-the-wall $U^+ = z^+$ and $U^+ = \frac{1}{\kappa} log\, z^+ + B$.

3.1 Velocity Profiles. Figure 4 depicts the double-averaged streamwise velocity from DERM as well as DNS for comparison. Visually it should be clear that the six surfaces investigated here give rise to markedly different velocity profiles. Overall, strong agreement is observed both above and below the roughness crests across the case matrix, for both rough wall–smooth wall and rough wall–rough wall configurations.

In Fig. 5, the double-averaged Reynolds stress $\langle R_{xz} \rangle^+$ and dispersive stress $\langle D_{xz} \rangle^+$ profiles are plotted for both DERM and DNS. First, we note that the dispersive stress values predicted by our neural network provide generally good agreement. A few pathologies are observable in the DERM predictions, particularly that the model has a tendency to underpredict the maximum value of dispersive stress in the roughness occupied region. These stress profiles

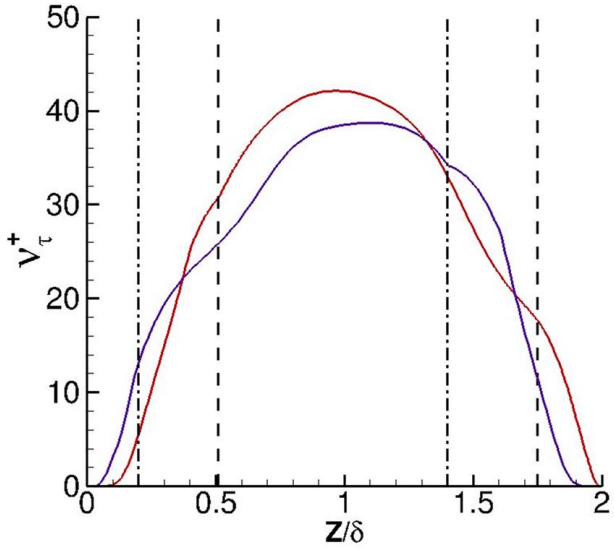

Fig. 8 Eddy viscosity profile for d/s and u/d (colors same as Fig. 4). Normalized by kinematic viscosity. Dashed lines show the match height z_m for d/s, and dashed dotted lines for u/d.

illustrate the necessity of including a dispersion model, particularly for channels including the *real* surface. Indeed, $\langle D_{xz} \rangle^+$ accounts for almost 25% of the stress balance at the height of the roughness and is of equivalent value to the Reynolds stress through roughly half of the roughness occupied layer. Failure to account for this component of the stress budget would have dramatically altered the DERM mean velocity profile.

The Reynolds stress predictions also accord well with the DNS, although there is a slight underprediction of the Reynolds stress in the roughness occupied layer for all three *real* surfaces (Figs. 5(*c*), (*e*), and (*f*)). The overall strong agreement across the case matrix demonstrates two things. First, it shows the accuracy of the predicted value of d provided by the sheltering model. Second, it confirms that, despite the nuances of AM channels, and with only minor modifications, existing DERM mixing length models remain a viable closure method.

Table 2 Drag partition

Case ID	f_{bot}, DERM	f_{bot}, DNS	f_{top}, DERM	f_{top}, DNS
u/s	56.6%	55.5%	43.4%	44.5%
d/s	67.1%	68.2%	32.9%	31.8%
r/s	75.2%	77.8%	24.8%	22.2%
u/d	37.1%	37.2%	62.9%	62.8%
u/r	26.7%	25.6%	73.3%	74.4%
d/r	38.3%	36.4%	61.7%	63.6%

Figures 6 and 7 show the velocity profiles for the top and bottom surfaces plotted in inner units. We observe the expected logarithmic behavior in the velocity profiles above the roughness heights, and we confirm that all three smooth surfaces conform to the law-of-the-wall despite the presence of rough surface on the opposite wall [29].

3.2 Eddy Viscosity. Figure 8 depicts the DERM profile of eddy viscosity for cases d/s and u/d. Here, we show that our two-layer approach transitions smoothly from calculating the eddy viscosity based on the mixing length, to determining it via the k-ε model. This applies for both the rough wall side and the smooth-wall side and underscores one of the benefits of the two-layer formulation.

3.3 Drag Partition. Another relevant engineering quantity when investigating channel flows is the partition of the total drag

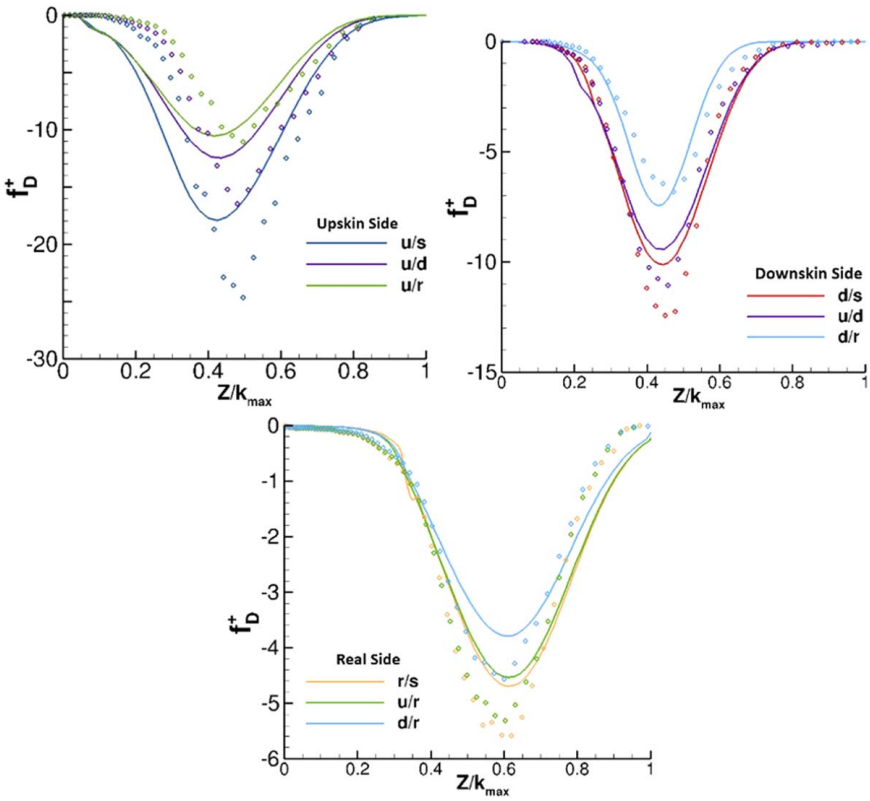

Fig. 9 The DERM drag force profiles for top: *upskin*, middle: *downskin*, and bottom: *real*. Solid lines correspond to DERM. Symbols are DNS. f_D^+ is normalized by $u_{\tau,N}^2/\delta$.

force between the top and bottom surfaces. These values can be computed directly from DERM, using an almost identical expression to the calculation of the total friction velocity given in Eq. (9). This expression is valid for both rough and smooth walls in the context of DERM, because in the smooth-wall case, f_D is zero and the drag on the surface is due only to viscous wall shear stress.

It should be noted that, by definition, the sum of the forces exerted by both the top and bottom walls should balance the total body force driving the flow. Because the total force driving the flow is given by $\int_0^{L_z} \beta(z) f_B \, dz$, and the volume fraction distribution is different for all six cases, the total driving forces will also be different.

Table 2 lists the drag partition as a percentage of the total drag for the top and bottom walls for all six cases. Unsurprisingly, given the performance of the stress budget predictions, all cases return the drag partition within roughly 3% of the DNS value. These values can be easily converted into a skin friction coefficient, which is useful in some contexts, although this is not done here.

Another way to characterize the DERM drag predictions is by examining the average drag profiles as a function of the wall normal location. Figure 9 compares DERM drag force to the DNS for the *upskin*, *downskin*, and *real* surface. Since each surface appears three times in the case matrix, each plot contains three set of curves. We make several observations about these data.

First DERM does not predict with high accuracy the drag contribution from the lowest regions of the roughness. For the *upskin* surfaces, for example, an overprediction of the drag near the wall accounts for the under prediction of the mean velocity in the bottom region of the roughness and the overprediction we observe near the roughness crest in Fig. 4.

This is not entirely surprising. The flow in the recesses of a rough surface is often recirculating, and the mean flow can even be in the negative direction, complicating simple modeling. In addition, the assumption of an exponential mean velocity profile in the roughness layer, which is a significant part of our drag sheltering model, is known to break down in the bottom layer of the roughness. This is mitigated by the fact that for this class of surface, the bottom 20% of the roughness layer contributes only about 5% of the total force budget, which is why the drag partition predictions are accurate, despite DERM not matching the exact force distribution. Additionally, because both β and A_f used in the DERM model are analytical curve fits for the exact roughness field, there is some error associated with their use, especially near the top and bottom of the roughness, which has some impact upon these results. Overall, the shape of the drag profiles are consistent with the DNS and follow the appropriate trends.

4 Conclusion

AM has expanded the design space for internal cooling channels in turbomachinery applications. In order to leverage this technology, designers will need predictive areo-thermal tools with resource requirements far lower than roughness resolving CFD. In this study, a volumetric roughness model, DERM, was presented and applied to a set of highly rough additively manufactured flow channels. The predictive capability of this model was demonstrated by comparing it to DNS results.

We have highlighted the importance of the dispersive stress in this class of roughness. Unlike other topologies, AM channels require a model to account for these stresses, and a data-based approach for closure was presented. The distribution of the drag force in the roughness occupied region is an area that calls for additional attention, although the integrated force is well predicted. Finally, it is noteworthy that closure of the Reynolds stress term with a mixing length model proved sufficiently accurate. This can be achieved without significant deviation from previously established forms of the mixing length, despite the complexity of the roughness field. Future work will involve incorporating a larger set of training data into the dispersion modeling network, and extending the model to surfaces with heat transfer.

Acknowledgment

This material is based upon work supported by the Department of Energy under Award Number(s) DE-FE0001730. Disclaimer: This report was prepared as an account of work sponsored by an agency of the United States Government. Neither the United States Government nor any agency thereof, nor any of their employees, makes any warranty, express or implied, or assumes any legal liability or responsibility for the accuracy, completeness, or usefulness of any information disclosed, or represents that its use would not infringe privately owned rights. The views and opinions of authors expressed herein do not necessarily state or reflect those of the United States Government or any agency thereof.

Conflict of Interest

There are no conflicts of interest.

Data Availability Statement

The datasets generated and supporting the findings of this article are obtainable from the corresponding author upon reasonable request.

Nomenclature

a = attenuation parameter
d = displacement height
k = turbulent kinetic energy
p = pressure
x = streamwise coordinate
z = Wall normal coordinate
H = boundary layer height
U = streamwise velocity
$\hat{z}$ = corrected wall distance
a_o = minimum attenuation parameter
f_b = volumetric body force
f_D = DERM drag force
k_{krt} = kurtosis of roughness height
k_m = mean roughness height
$k_{\max}$ = maximum height of roughness
k_{rms} = root-mean-squared roughness height
l_m = turbulent mixing length
$l_{m,i}$ = roughness layer mixing length
$l_{m,o}$ = outer layer mixing length
$u_{\tau,N}$ = nominal friction velocity
$u_{\tau,T}$ = total friction velocity
z_o = hydrodynamic roughness length
z_m = eddy viscosity match height
A_f = projected frontal area
C_D = sectional drag coefficient
C_o = isolated drag coefficient
D_{ij} = dispersive stress tensor
L_z = wall-normal domain height
R_{ij} = Reynolds stress tensor
U_k = mean velocity at roughness crest
ES = element slope parameter
β = volume fraction $\forall_f/\forall$
δ = half channel height
ε = turbulent dissipation rate
κ = von Karman constant
ν = kinematic viscosity
ν_τ = eddy viscosity
ρ = density
σ_k = roughness height standard deviation
τ_w = wall shear stress
ϕ = generic variable
$\forall$ = volume

$\cdot''$ = spatially fluctuating quantity
$\cdot'$ = temporally fluctuating quantity
$\bar{\cdot}$ = time-averaged quantity
$\langle \cdot \rangle$ = comprehensive spatial average
$\langle \cdot \rangle^f$ = intrinsic spatial average

References

[1] Snyder, J. C., Stimpson, C. K., Thole, K. A., and Mongillo, D., 2016, "Build Direction Effects on Additively Manufactured Channels," ASME J. Turbomach., **138**(5), p. 051006.
[2] Snyder, J. C., Stimpson, C. K., Thole, K. A., and Mongillo, D., 2015, "Build Direction Effects on Microchannel Tolerance and Surface Roughness," ASME J. Turbomach., **137**(11), p. 111411.
[3] Stimpson, C. K., Snyder, J. C., Thole, K. A., and Mongillo, D., 2016, "Roughness Effects on Flow and Heat Transfer for Additively Manufactured Channels," ASME J. Turbomach., **138**(5), p. 051008.
[4] Stimpson, C. K., Snyder, J. C., Thole, K. A., and Mongillo, D., 2017, "Scaling Roughness Effects on Pressure Loss and Heat Transfer of Additively Manufactured Channels," ASME J. Turbomach., **139**(2), p. 021003.
[5] Kirsch, K. L., and Thole, K. A., 2018, "Numerical Optimization, Characterization, and Experimental Investigation of Additively Manufactured Communicating Microchannels," ASME J. Turbomach., **140**(11), p. 111003.
[6] Hanson, D. R., McClain, S. T., Snyder, J. C., Kunz, R. F., and Thole, K. A., 2019, "Flow in a Scaled Turbine Coolant Channel With Roughness Due to Additive Manufacturing," Proceedings of ASME Turbo Expo 2019, Phoenix, AZ, June 17–21, pp. 1–12.
[7] Flack, K. A., and Schultz, M. P., 2014, "Roughness Effects on Wall-Bounded Turbulent Flows," Phys. Fluids, **26**(10), p. 101305.
[8] Schultz, M. P., and Flack, K. A., 2008, "Turbulent Boundary Layers on a Systematically Varied Rough Wall," Phys. Fluids, **21**(1), pp. 1–9.
[9] Flack, K. A., and Schultz, M. P., 2010, "Review of Hydraulic Roughness Scales in the Fully Rough Regime," ASME J. Fluids Eng., **132**(4), p. 041203.
[10] Bons, J. P., McClain, S. T., Wang, Z. J., Chi, X., and Shih, T. I., 2008, "A Comparison of Approximate Versus Exact Geometrical Representations of Roughness for CFD Calculations of C_f and S_t," ASME J. Turbomach., **130**(2), p. 021024.
[11] Schlicting, H., 1936, "Experimental Investigation of the Problem of Surface Roughness," NACA TM823.
[12] Taylor, R. P., Coleman, H. W., and Hodge, B. K., 1985, "Prediction of Turbulent Rough-Wall Skin Friction Using a Discrete Element Approach," ASME J. Fluids Eng., **107**(2), pp. 251–257.
[13] Taylor, R. P., Coleman, H. W., and Hodge, B. K., 1983, *AFATL Technical Report 83-90*, Harvard, Cambridge, MA.
[14] Taylor, R. P., Coleman, H. W., and Hodge, B. K., 1989, "Prediction of Heat Transfer in Turbulent Flow Over Rough Surfaces," ASME J. Heat Mass Trans., **111**(2), pp. 568–572.
[15] McClain, S., 2002, "A Discrete-Element Model for Turbulent Flow Over Randomly Rough Surfaces," Ph.D. thesis, Mississippi State University, MS
[16] McClain, S. T., Hodge, B. K., and Bons, J. P., 2004, "Predicting Skin Friction and Heat Transfer for Turbulent Flow Over Real Gas Turbine Surface Roughness Using the Discrete Element Method," ASME J. Turbomach., **126**(2), pp. 259–267.
[17] McClain, S. T., and Brown, J. M., 2009, "Reduced Rough-Surface Parametrization for Use With the Discrete-Element Model," ASME J. Turbomach., **131**(2), pp. 75–84.
[18] Aupoix, B., 1994, "Modeling of Boundary Layers Over Rough Surfaces," Advances in Turbulence V: Proceedings of the Fifth European Turbulence Conference, Siena, Italy, July 5–8, pp. 16–20.
[19] Whitaker, S., 1986, "Flow in Porous Media I: A Theoretical Derivation of Darcy's Law," Trans. Porous Media, **1**(3), pp. 3–25.
[20] Crapiste, G., Rotstein, E., and Whitaker, S., 1986, "A General Closure Scheme for the Method of Volume Averaging," Chem. Eng. Sci., **41**(2), pp. 227–235.
[21] Pedras, M., and de Lemos, M., 2001, "Macroscopic Turbulence Modeling for Incompressible Flow Through Undeformable Porous Media," Int. J. Heat Mass Transfer, **44**(6), pp. 1081–1093.
[22] Aupoix, B., 2016, "Revisiting the Discrete Element Method for Predictions of Flows Over Rough Surfaces," ASME J. Fluids Eng., **138**(3), p. 031205.
[23] Hanson, D. R., 2017, "Computational Investigation of Convective Heat Transfer on Ice-roughened Aerodynamic Surfaces," Ph.D. thesis, Pennsylvania State University, PA.
[24] Hanson, D. R., Kinzel, M. P., and McClain, S. T., 2019, "Validation of the Discrete Element Roughness Method for Predicting Heat Transfer on Rough Surfaces," Int. J. Heat. Mass. Transfer., **136**(6), pp. 1217–1232.
[25] Hanson, D. R., and Kinzel, M. P., 2019, "Evaluation of a Subgrid-Scale Computational Fluid Dynamics Model for Ice Roughness," AIAA J. Aircraft, **56**(2), pp. 787–799.
[26] Chedevergne, F., and Forooghi, P., 2020, "On the Importance of the Drag Coefficient Modelling in the Double Averaged Navier-Stokes Equations for Prediction of the Roughness Effects," J. Turbul., **21**(8), pp. 463–482.
[27] McClain, S. T., Hanson, D. R., Cinnamon, E., Snyder, J. C., Kunz, R. F., and Thole, K. A., 2021, "Flow in a Simulated Turbine Blade Cooling Channel With Spatially Varying Roughness Caused by Additive Manufacturing Orientation," ASME J. Turbomach., **143**(7), p. 071013.
[28] Stafford, G. J., McClain, S. T., Hanson, D. R., Kunz, R. F., and Thole, K. A., 2022, "Convection in Scaled Turbine Internal Cooling Passages With Additive Manufacturing Roughness," ASME J. Turbomach., **144**(4), p. 041008.
[29] Altland, S. J., Zhu, X., McClain, S. T., Kunz, R. F., and Yang, X. I. A., 2021, "Flow in Additively Manufactured Super Rough Channels," J. Flow, **2**, p. E19.
[30] Raupach, M., 1992, "Drag and Drag Partition on Rough Surfaces," Boundary Layer Meteorol., **60**, pp. 1–25.
[31] Yang, X. I. A., Sadique, J., Mittal, M., and Meneveau, C., 2016, "Exponential Roughness Layer and Analytical Model for Turbulent Boundary Layer Flow Over Rectangular-Prism Roughness Elements," J. Fluid Mech., **789**, pp. 127–165.
[32] McClain, S. T., Collins, S. P., Hodge, B. K., and Bons, J. P., 2006, "The Importance of the Mean Elevation in Predicting Skin Friction for Flow Over Closely Packed Surface Roughness," ASME J. Fluids Eng., **128**(3), pp. 579–586.
[33] Nikuradse, J., 1937, "Law of Flow in Rough Pipes," NACA, WA, Technical Memorandum 1292.
[34] Antonialli, I. A., and Silveira-Neto, A., 2018, "Theoretical Study of Fully Developed Turbulent Flow in a Channel, Using Prandtl's Mixing Length Model," J. Appl. Mathe. Phys., **6**(4), pp. 677–692.
[35] Launder, B. E., and Spalding, D. B., 1974, "The Numerical Computation of Turbulent Flows," Comput. Methods. Appl. Mech. Eng., **3**(2), pp. 269–289.
[36] Kuwata, Y., and Kawaguchi, Y., 2018, "Direct Numerical Simulation of Turbulence Over Systematically Varied Irregular Rough Surfaces," J. Fluid Mech., **862**, pp. 781–815.
[37] Jelly, T. O., and Busse, A., 2019, "Reynolds Number Dependence of Reynolds and Dispersive Stresses in Turbulent Channel Flow Past Irregular Near-Gaussian Roughness," Int. J. Heat Fluid Flow, **80**, p. 108485.
[38] Busse, A., and Jelly, T. O., 2020, "Influence of Surface Anisotropy on Turbulent Flow Over Irregular Roughness," Flow, Turbulence Combust., **104**, pp. 331–354.
[39] Yang, X. I. A., Zafar, S., Wang, J. X., and Xiao, H., 2019, "Predictive Large-Eddy-Simulation Wall Modeling Via Physics-Informed Neural Networks," Phys. Rev. Fluids, **4**, p. 034602.
[40] Chung, D., Hutchins, N., Schults, M., and Flack, K., 2021, "Predicting the Drag of Rough Surfaces," Annu. Rev. Fluid Mech., **53**, pp. 439–471.
[41] Xu, H., Altland, S., Yang, X., and Kunz, K., 2021, "Flow Over Closely Packed Cubical Roughness," J. Fluid Mech., **920**, pp. 1–24.
[42] Levenberg, K., 1944, "A Method for the Solution of Certain Non-linear Problems in Least Squares," Q. Appl. Math, **2**(2), pp. 164–168.
[43] Altland, S., 2022, "A Distributed Element Roughness Model Based on the Double Averaged Navier-Stokes Equations," Ph.D. thesis, Pennsylvania State University, PA.
[44] Kunz, R. F., 2001, "An Unstructured Two-Fluid Method Based on the Coupled Phasic Exchange Algorithm," 15th AIAA Computational Fluid Dynamics Conference, Anaheim, CA, June 11–14, p. 2672.